METEOROLOGICAL OFFICE
130436
25 SEP 1979
LIBRARY

MET O 11 TECHNICAL NOTE NO. 129

STRATOCUMULUS

by

R N B Smith

Met O 11
Meteorological Office
London Road
Bracknell
Berkshire
United Kingdom

N.B This paper has not been published. Permission to quote from it must be obtained from the Assistant Director in charge of the above Met Office Branch.

September 1979

FH2A

MET O 11 TECHNICAL NOTE NO. 129

STRATOCUMULUS

by R N B Smith

SUMMARY

A review of recent studies of the physics of stratocumulus clouds is presented. After a brief desription of the main features of stratocumulus, the basic equations and assumptions required for one-dimensional and three-dimensional models are discussed. The predictions of such models are also included.

1. INTRODUCTION

Stratocumulus (Sc) is layer cloud in the lower atmosphere that has internal structure such as denser regions, convective rolls and cells and also surface irregularities such as domes and wisps. It is this structure which distinguishes stratocumulus from stratus, which is uniform.

There is a purely scientific interest in understanding the formation, maintainance and dissipation of stratocumulus. There is also a need to use this understanding in day-to-day forecasting practice. The presence of Sc can affect surface visibility, th formation of fog or frost and even the surface wind.

With the continuing development of NWP models, both on the synoptic and meso scales, accurate but simple ways of computing the sub-grid fluxes of momentum, heat and moisture in terms of the grid variables are required. These "parametrizations" can be formulated confidently only when the physical processes in the atmospheric boundary layer are understood. The formation, maintainance and dissipation of Sc are frequently occurring examples of such processes. The study of stratocumulus is therefore important for the formulation of NWP models.

It is the purpose of this note to review current knowledge about stratocumulus and to discuss some models which have been used to investigate its structure in a quantitative manner.

2. THE MAIN FEATURES OF STRATOCUMULUS

2.1 The Observed features of stratocumulus

Cornford (1966) has reviewed and commented on several observational studies of stratocumulus and further details of the topics in this section can be found there.

Temperature There is usually a marked inversion at cloud top. Temperature increases of up to 8K over a depth of 100m have been observed (James (1959), Moore (1964)). Above the inversion there is a stable or neutral temperature lapse rate.

Humidity Associated with the temperature inversion there is a sharp decrease with height in the specific humidity. Most of the decrease again occurs over a depth of 100 m (James (1959), Moore (1964)). It has been observed that the humidity below the cloud layer can decrease with height. A plausible explanation for this is that the convective turbulence maintaining the stratocumulus may not always be driven by heating from the ground. In these circumstances the mixing, which tends to homogenize conservative quantities, may not reach down to the ground. However, it is also possible that the sub-cloud humidity gradient persists despite the convection and enhances upward transport of water vapour.

Liquid Water Content This is observed to follow the adiabatic value near the base of the cloud but falls away near the cloud top.

Turbulence The stratocumulus layer and the sub-cloud layer are turbulent but the intensity of the turbulence falls almost to zero above the inversion.

Radiation Measurements of long-wave radiation flux through a stratocumulus sheet

indicate a net cooling of the cloud near its top. This can often be the main cause of turbulence in stratocumulus cloud. There can also be a relatively weak heating of the cloud base by long-wave radiation from the ground.

Other Features Holes in otherwise continuous stratocumulus are sometimes found downwind of hills as a result of orographically forced waves in the cloud sheet. The shape of the cloud top, which determines the depth of the layer in which exchanges between clear and cloudy air occur, appears to be related to the amount of radiative cooling and the stability of the air in and above the cloud.

2.2 The Occurence of Stratocumulus

Stratocumulus is found in a variety of climatic conditions.

Sub-tropical trade wind Sc forms over warm oceans and can persist for several days. Nearer the tropics it may break up into isolated cumuli. The inversion, beneath which the cloud forms, is initially a subsidence inversion in the descending portion of the tropical Hadley cell (Schubert (1976)).

Anticyclonic Sc is often found in mid and high latitudes and is similar to the trade wind Sc, the subsidence being that associated with the anticyclone. Findlater (1961) found that stratocumulus in these conditions was confined to colder areas of air while in the relatively warmer air the skies were clear. His analyses showed that these cold and warm areas were the remnants of different air masses which had retained their identity after the fronts separating them had been omitted from the routine analyses.

Sc over sea bordering hot dry climates Stratocumulus occurs over the cool eastern oceans in the subsidence to the east of subtropical oceanic high pressure cells. The sea is cool because of upwelling currents and, although a source of moisture, does not heat the overlying air. The convective turbulence is driven by the radiative cooling at the cloud top. A review of the climatology of these areas is given by Schubert et al. (1977).

Arctic Sc often develops from stratus over the Arctic oceans and beneath the intense Arctic inversions.

3. ONE - DIMENSIONAL MODELS OF STRATOCUMULUS

3.1 Basic Equations

The starting point in the formulation of 1-d models is the set of balance equations for specific humidity, q, cloud water concentration, c and potential temperature θ. These are, respectively,

$$\frac{\partial q}{\partial t} + \underset{\sim}{v}_H \cdot \nabla q + w\frac{\partial q}{\partial z} = -S - \frac{1}{\rho}\frac{\partial}{\partial z}\left(\rho \overline{w'q'}\right) \qquad (3.1)$$

$$\frac{\partial c}{\partial t} + \underset{\sim}{v}_H \cdot \nabla c + w\frac{\partial c}{\partial z} = S - \frac{1}{\rho}\frac{\partial}{\partial z}\left(\rho \overline{w'c'}\right) \qquad (3.2)$$

$$\frac{\partial \theta}{\partial t} + \underline{v}_H \cdot \nabla \theta + w \frac{\partial \theta}{\partial z} = \frac{1}{c_p P}(Q + LS) - \frac{1}{\rho}\frac{\partial}{\partial z}\left(\rho \overline{w'\theta'}\right) \qquad (3.3)$$

The unprimed variables are large scale averages with a horizontal scale much larger than that of all the convective overturning motions in the boundary layer. Primes denote small scale deviations from the averages and the overbars the average of the expressions beneath them.

The large scale velocity $\underline{v}$, the Exner function $P = (p/p_r)^{R/c_p}$ and density ρ are assumed given. S is the microphysical source term for cloud water and Q is the source of radiational heat per unit mass of air.

It is convenient to introduce (following Deardorff (1976)) the equivalent potential temperature, θ_e, given by

$$\theta_e = \theta + \frac{L}{c_p P} q$$

and the total water concentration q_w defined by

$$q_w = \begin{cases} q & \text{if } q < q^* \\ q^* + c & \text{if } q \geq q^* \end{cases}$$

where q^* is the saturation specific humidity. To the extent that L/P is effectively constant in comparison with q we can deduce from (3.1) and (3.3) that

$$\frac{\partial \theta_e}{\partial t} + \underline{v}_H \cdot \nabla \theta_e + w \frac{\partial \theta_e}{\partial z} = \frac{-1}{c_p P}\frac{1}{\rho}\frac{\partial}{\partial z}(\rho R) - \frac{1}{\rho}\frac{\partial}{\partial z}\left(\rho \overline{w'\theta_e'}\right) \qquad (3.4)$$

where ρR is the radiative flux per unit volume. From (3.1) and (3.2) we have

$$\frac{\partial q_w}{\partial t} + \underline{v}_H \cdot \nabla q_w + w \frac{\partial q_w}{\partial z} = -\frac{1}{\rho}\frac{\partial}{\partial z}\left(\rho \overline{w'q_w'}\right) \qquad (3.5)$$

The advantage of (3.4) and (3.5) is that no terms representing change of state or latent heat release occur in them. This is equivalent to saying that θ_e and q_w are conserved in phase changes.

All 1-d models of stratocumulus (Lilly (1968), Schubert (1976), Deardorff (1976b) and Schubert et al (1977)) are based on equations (3.4) and (3.5).

3.2 The formulation of a one-dimensional model

From the discussion of the main features of stratocumulus in § 2.1 we can build up a primitive picture of the physical processes and structure in the cloud. The mathematical modelling of these processes, suitably idealized, is reviewed in this section.

The general balance of physical processes in and near stratocumulus cloud is set out diagramatically in Figure 1. We assume that the air above the surface layer and

below the lowest excursions of the cloud top is well mixed by the convective turbulence. Therefore there are no vertical gradients of conservative quantities in this layer.

Apart from the radiative contributions to the energy budget, heat can be transported into the mixed layer by the turbulence from the surface layer and from the stable air above the cloud, which is entrained. This latter process will be discussed in detail below.

The assumed profiles for θ_e, q_w and R are shown in Figure 2. In this figure z_T is the height above which turbulence is negligible and h is the height of the mixed layer. The values of θ_e and q_w are assumed to change rapidly across the layer $h \leq z \leq z_T$.

Idealised profiles of the long-wave radiative fluxes and resultant heating rate are depicted in Figure 3. The flux profile is also shown in Figure 2. The jump in radiative flux at the cloud top, which is associated with the cooling there, takes place in the layer $z_B \leq z \leq z_T$. Note that the possibility of some of this cooling occuring in the mixed layer has been allowed for by assuming that $z_B < h$.

3.2.1 Turbulent Flux Profiles Using the fact that θ_e and q_w are assumed constant with height in the mixed layer $0 \leq z \leq h$, it follows from (3.4) and (3.5) that the vertical fluxes $\overline{w'\theta_e'}$ and $\overline{w'q_w'}$ are linear with height and therefore given by

$$\overline{w'\theta_e'} = \left(1-\frac{z}{h}\right)\left(\overline{w'\theta_e'}\right)_0 + \frac{z}{h}\left\{\left(\overline{w'\theta_e'}\right)_h + \frac{(1-r)}{P_h}\Delta R\right\} \qquad 0 \leq z \leq z_B \qquad (3.6)$$

$$\overline{w'q_w'} = \left(1-\frac{z}{h}\right)\left(\overline{w'q_w'}\right)_0 + \frac{z}{h}\left(\overline{w'q_w'}\right)_h \qquad 0 \leq z \leq h \qquad (3.7)$$

$\left(\overline{w'\theta_e'}\right)_0$ and $\left(\overline{w'q_w'}\right)_0$ are the respective values of $\overline{w'\theta_e'}$ and $\overline{w'q_w'}$ at the top of the surface layer. ΔR is the total radiative flux difference pertaining to the layer $z_B \leq z \leq z_T$. r is the fraction of this cooling which occurs in the inversion layer $h \leq z \leq z_T$. Lilly (1968) and Schubert (1976) and (1977) tacitly assume that $r = 1$. Note that the quantity $\overline{w'\theta_e'}$ jumps from $\left(\overline{w'\theta_e'}\right)_h + \frac{(1-r)\Delta R}{P_h}$ to $\left(\overline{w'\theta_e'}\right)_h$ in the thin layer $z_B \leq z \leq h$.

3.2.2 Cloud Top Jump Conditions

If (3.4) and (3.5) are integrated over the thin inversion layer we obtain, using the rule for differentiating an integral with variable limits,

$$W_e \Delta\theta_e = \frac{r\Delta R}{P_h} - \left(\overline{w'\theta_e'}\right)_h \qquad (3.8)$$

$$W_e \Delta q_w = -\left(\overline{w'q_w'}\right)_h. \qquad (3.9)$$

Here $\Delta\theta_e$, Δq_w are the jumps in θ_e, q_w occuring in the inversion layer and We, the entrainment rate, is given by

$$W_e = \frac{\partial h}{\partial t} + \underline{v}_H \cdot \nabla h - w_h \qquad (3.10)$$

where w_h is the large scale vertical velocity at the top of the mixed layer.

3.2.3 Surface Fluxes

The turbulent fluxes at the top of the surface layer have to be specified by surface layer theory. Schubert et al (1977) in their model of marine stratocumulus use the relations

$$\left(\overline{w'\theta_e'}\right)_0 = cV\left(\theta_{es}^* - \theta_{eM}\right) \qquad (3.11)$$

$$\left(\overline{w'q_w'}\right)_0 = cV\left(q_s^* - q_{wM}\right) \qquad (3.12)$$

where c is a bulk transfer coefficient, V is the surface wind speed, θ_{es}^* and q_s^* are the saturation values of θ_e and q at the sea surface temperature and θ_{eM}, q_{wM} are the mixed layer values of θ_e, q_w.

3.2.4 Radiative Cooling

The cloud top radiative cooling rate ΔR can either be given independently as a function of time (Schubert (1976)) or, more realistically, given by a radiative model coupled to the convective model (Schubert et al (1977)).

ΔR is the sum of a small cloud top jump in short-wave solar radiation ΔR_s, a given function of time, and the more important jump in long-wave radiation $\Delta R_L = F^{\uparrow}(z_T) - F^{\downarrow}(z_T)$. The downward flux of long-wave radiation onto the cloud top $F^{\downarrow}(z_T)$ can be assumed given and the upward flux from the cloud top is given by the black-body relation

$$F^{\uparrow}(z_T) = \sigma T^4(h^-) \qquad (3.13)$$

$T(h^-)$ is the cloud top temperature which has to be related to the model variables θ_{eM}, q_{wM} etc.

Now

$$T(h^-) = P_h\,\theta(h^-) = P_h\left[\theta_{eM} - \frac{L}{c_p P_h}\,q(h^-)\right]$$

$$= P_h\,\theta_{eM} - \frac{L}{c_p}\,q^*(h^-) \qquad (3.14)$$

Noting that $q^*(z_c) = q_{wM}$, $q^*(h^-)$ can be computed from the approximate relation

$$q^*(h^-) = \left(\frac{\partial q^*}{\partial z}\right)_{\theta_e}(h - z_c) + q_{wM} \qquad (3.15)$$

where $(\partial q^*/\partial z)_{\theta_e}$ is the lapse rate of the saturated specific humidity following a wet adiabat.

3.2.5 The Height of the Cloud Base

The cloud base height occuring in equation (3.15) is given by

$$z_c = (q_{wm} - q_o^*) \Big/ \left(\frac{\partial q}{\partial z}\right)_\theta \qquad (3.16)$$

where q_o^* is the saturated specific humidity at $z=0$ and $(\partial q/\partial z)_\theta$ is its lapse rate following an adiabat.

3.2.6 Entrainment at the Cloud Top

In order to close the system of equations of the model we need to relate the turbulent fluxes at $z=h$ to the model variables. Such a relation is known as an entrainment hypothesis because it allows the entrainment rate to be found from equations (3.8) and (3.9).

From a theoretical standpoint the closure should be effected by specifying the turbulent energy balance in the mixed layer. Then, in principle, we could obtain a relationship between the turbulent fluxes at the top of the layer and the turbulent kinetic energy available for entrainment. A discusssion of this approach is given by Stull (1976).

The balance equation for turbulent kinetic energy $\bar{E}$ can be written as

$$\frac{D\bar{E}}{Dt} = -\frac{1}{\rho}\frac{\partial}{\partial z}\left(\rho\,\overline{w'(E + c_p\theta P')}\right) + \frac{g}{\theta_o}\overline{w'\theta_v'} - (\overline{w'\underline{v}'}).\frac{\partial \underline{v}}{\partial z} - \varepsilon \qquad (3.17)$$

where θ_v' is the perturbation virtual potential temperature given by

$$\theta_v' = \theta' + \theta_o(0.61q' - c')$$

ε is the rate of dissipation of turbulent kinetic energy to thermal energy by molecular viscous forces. The second term on the r.h.s gives the rate of turbulent energy generation by buoyancy and the third term gives the rate of generation by mechanical means.

Integrating (3.17) from $z=0$ to $z=z_T$ we obtain

$$\int_0^{z_T}\frac{D\bar{E}}{Dt}\,dz = -\left[\overline{w'(E + c_p\theta P')}\right]_0^{z_T} - \int_0^{z_T}\overline{w'\underline{v}'}.\frac{\partial \underline{v}}{\partial z} + \int_0^{z_T}\frac{g}{\theta_o}\overline{w'\theta_v'}\,dz - \int_0^{z_T}\varepsilon\,dz \qquad (3.18)$$

The definition of z_T ensures that negligible energy is transported vertically at $z=z_T$ by gravity waves. The first term on the r.h.s of (3.18) therefore contributes

nothing. The equation is complex and several conjectures have to be made to reduce it to a form simple enough for our purpose. The simplest reduction of (3.18) is

$$\frac{g}{\theta_0}\int_0^{z_T} \overline{w'\theta_v'}\, dz - \int_0^{z_T} \varepsilon\, dz = 0 \qquad (3.19)$$

(3.19) follows from (3.18) by assuming that:

(i) the turbulence is steady and homogeneous so that the l.h.s of (3.18) is zero;

(ii) mechanical production of turbulent energy is negligible.

Splitting the buoyancy flux integral in (3.19) into the positive part over the mixed layer and the negative part over the inversion layer (see Figure 2) we get

$$\frac{g}{\theta_0}\int_0^{h} \overline{w'\theta_v'}\, dz + \frac{g}{\theta_0}\int_h^{z_T} \overline{w'\theta_v'}\, dz - \int_0^{z_T} \varepsilon\, dz = 0 \qquad (3.20)$$

If it is now assumed that $\varepsilon \simeq 0$ for $z > h$ and that the rate of dissipation in the mixed layer is a fixed fraction $f < 1$ of the turbulent energy production rate, ie

$$\int_0^h \varepsilon\, dz = f \int_0^h \frac{g}{\theta_0} \overline{w'\theta_v'}\, dz,$$

then

$$\int_h^{z_T} \overline{w'\theta_v'}\, dz = -(1-f)\int_0^h \overline{w'\theta_v'}\, dz \qquad (3.21)$$

The integral on the l.h.s of (3.21) can be approximated by

$$\int_h^{z_T} \overline{w'\theta_v'}\, dz \simeq \frac{(z_T - h)}{2}\left(\overline{w'\theta_v'}\right)_h.$$

So (3.21) becomes

$$\left(\overline{w'\theta_v'}\right)_h = -A\int_0^h \overline{w'\theta_v'}\, dz/h \qquad (3.22)$$

where A is given by $A = 2(1-f)h/(z_T - h)$ and is assumed constant. It is conventional to write $A = 2h/(1-k)$ where k is called the entrainment parameter. With this notation we can rewrite (3.22) as

$$\left(\overline{w'\theta_v'}\right)_h = \frac{-2k}{(1-k)}\int_0^h \overline{w'\theta_v'}\, dz/h \qquad (3.23)$$

In order that the turbulence is maintained we must have

$$I \equiv \int_0^h \overline{w'\theta_v'}\, dz/h > 0.$$

Because of the number of assumptions and approximations involved, the discussion leading up to equation (3.23) should not be regarded as a derivation. Instead (3.23) is best regarded as an hypothesis which is demonstrated to be plausible by the argument presented.

The 1-d model of Schubert (1976) and (1977), the predictions of which will be discussed later, uses a slightly different entrainment hypothesis in place of (3.23). Schubert puts

$$(\overline{w'\theta_v'})_{min} = \frac{-2k}{(1-k)} I \qquad (3.24)$$

and does not assume that the minimum value of the buoyancy flux occurs at $z = h$. However, if a value of r less than 1 is assumed, $\overline{w'\theta_v'}$ has a negative jump of magnitude $(1-r)\Delta R/P_h$ just below $z=h$ and this probably ensures that $(\overline{w'\theta_v'})_{min} = (\overline{w'\theta_v'})_h$. Schubert assumes r=1 and so does not have a double jump structure for the buoyancy flux.

3.2.7 The buoyancy flux profile

The entrainment hypothesis is the closure relation required for the model. However, (3.23) contains the buoyancy flux $\overline{w'\theta_v'}$ which we must write in terms of the heat and water fluxes which are given by (3.6) and (3.7). Details of this calculation can be found in Deardorff (1976b). The results are:

$$\overline{w'\theta_v'} = \overline{w'\theta_e'} - C_1\theta_0\overline{w'q_w'} \qquad 0 \leq z < z_c \quad \text{(the subcloud layer)} \qquad (3.25)$$

and $$\overline{w'\theta_v'} = C_2\overline{w'\theta_e'} - \theta_0\overline{w'q_w'} \qquad \text{for } z_c < z < h \quad \text{(the cloud layer)}$$

where

$$C_1 = \frac{L}{c_p P \theta_0} - 0.61$$

$$C_2 = \left[1 + 1.61\theta_0\left(\frac{0.622 L q_M^*}{R T_M \theta_M}\right)\right] \Big/ \left[1 + \frac{0.622 L^2 q_M^*}{R c_p T_M \theta_M P}\right]$$

Note that there is a discontinuity in $\overline{w'\theta_v'}$ at cloud base. The bouyancy flux profile is shown in Figure 2.

Equations (3.25) can be used to obtain an expression for I. We find

$$I = K_1(\overline{w'\theta_e'})_0 - K_2\theta_0(\overline{w'q_w'})_0 + K_3\left[(\overline{w'\theta_e'})_h + \frac{(1-r)\Delta R}{P_h}\right] - K_4\theta_0(\overline{w'q_w'})_h \qquad (3.26)$$

where the coefficients are given by

$$K_1 = \tfrac{1}{2} C_2 \left(1 - \tfrac{z_c}{h}\right)^2 + \tfrac{z_c}{h}\left(1 - \tfrac{z_c}{h}\right)$$

$$K_2 = \tfrac{1}{2} \left(1 - \tfrac{z_c}{h}\right)^2 + C_1 \tfrac{z_c}{h}\left(1 - \tfrac{z_c}{h}\right)$$

$$K_3 = \tfrac{1}{2} C_2 \left[1 - \left(\tfrac{z_c}{h}\right)^2\right] + \tfrac{1}{2}\left(\tfrac{z_c}{h}\right)^2$$

$$K_4 = \tfrac{1}{2} \left[1 - \left(\tfrac{z_c}{h}\right)^2\right] + \tfrac{1}{2} C_1 \left(\tfrac{z_c}{h}\right)^2$$

Equation (3.23) can now be rewritten as

$$\frac{(1-k)}{2k}\left\{\theta_o \left(\overline{w'q_w'}\right)_h - C_2 \left(\overline{w'\theta_e'}\right)_h\right\} = K_1 \left(\overline{w'\theta_e'}\right)_o - K_2 \theta_o \left(\overline{w'q_w'}\right)_o + K_3 \left\{\left(\overline{w'\theta_e'}\right)_h + \frac{(1-r)\Delta R}{P_h}\right\} - K_4 \theta_o \left(\overline{w'q_w'}\right)_h \qquad (3.27)$$

3.28 Summary of the 1-d model

A coupled convective-radiative 1-d model consists of the surface flux relations (3.11) and (3.12) (or some other relations for the surface layer over land), the cloud base height relation (3.16), the cloud-top temperature and radiation relations (3.14), (3.15) and (3.13), a consistency relation derived from (3.8) and (3.9) by eliminating We, the entrainment relation (3.27), the mixed layer budgets (3.4) and (3.5) and the cloud-top jump condition (3.8).

These equations are set out below in an appropriate order for numerical integration

$$\left(\overline{w'\theta_e'}\right)_o = cV\left(\theta_{es}^* - \theta_{eM}\right) \qquad (M.1)$$

$$\left(\overline{w'q_w'}\right)_o = cV\left(q_s^* - q_{wM}\right) \qquad (M.2)$$

$$\Delta\theta_e = \theta_e(z_T) - \theta_{eM} \qquad (M.3)$$

$$\Delta q_w = q(z_T) - q_{wM} \qquad (M.4)$$

$$z_c = \left(q_{wM} - q_s^*\right) \Big/ \left(\frac{\partial q^*}{\partial z}\right)_\theta \qquad (M.5)$$

$$T(h^-) = P_h \theta_{eM} - \frac{L}{c_p}\left\{\left(\frac{\partial q^*}{\partial z}\right)_{\theta_e}(h - z_c) + q_{wM}\right\} \qquad (M.6)$$

$$\Delta R = \sigma T^4(h^-) - F_L^{\downarrow}(z_T) + \Delta R_s \qquad (M.7)$$

$$\Delta q_w \left(\overline{w'\theta_e'}\right)_h - \Delta\theta_e \left(\overline{w'q_w'}\right)_h = \frac{r\Delta R \Delta q_w}{P_h} \qquad (M.8)$$

$$-\left\{K_3 + \frac{(1-k)}{2k} C_2\right\}\left(\overline{w'\theta_e'}\right)_h + \left\{K_4 + \frac{(1-k)}{2k}\right\}\theta_o \left(\overline{w'q_w'}\right)_h = \frac{K_3(1-r)\Delta R}{P_h} + K_1 \left(\overline{w'\theta_e'}\right)_o - K_2 \theta_o \left(\overline{w'q_w'}\right)_o \qquad (M.9)$$

$$\frac{d\theta_{eM}}{dt} = \frac{\{(\overline{w'\theta_e'})_o - (\overline{w'\theta_e'})_h - (1-r)\Delta R/\rho_h\}}{h} \qquad (M.10)$$

$$\frac{dq_{wM}}{dt} = \frac{\{(\overline{w'q_w'})_o - (\overline{w'q_w'})_h\}}{h} \qquad (M.11).$$

$$\frac{dh}{dt} = w_h + \frac{\{r\Delta R/\rho_h - (\overline{w'\theta_e'})_h\}}{\Delta\theta_e} \qquad (M.12)$$

The pair of equations (M.8) and (M.9) have to be solved simultaneously for $(\overline{w'\theta_e'})_h$ and $(\overline{w'q_w'})_h$. When these fluxes have been computed it should be checked that $I \geq 0$. With initial values of θ_{eM}, q_{wM} and h the system (M.1)–(M.2) can be integrated numerically with various sea surface temperatures, stable layer temperatures and humidities and large scale divergences.

3.2.9 Horizontally homogeneous steady state solutions

Schubert (1977) computes values of h by an iterative method from the horizontally homogeneous, steady state version of his model. The dependence of the various model outputs on the large-scale divergence and sea surface temperature is investigated. Schubert's main conclusions are that:

(1) the boundary layer is deeper when the large-scale divergence is smaller or when the sea surface temperature is greater. The depth h is approximately inversely proportional to the divergence D so the cloud-top subsidence rate $w_h = -Dh$ remains roughly the same;

(2) the cloud base height z_c is greater when the divergence is smaller or when the sea surface temperature is greater but the variation of z_c is much less than that of h;

(3) the upward long-wave flux of radiation from the top of the cloud is mainly influenced by the decrease in the cloud-top temperature as h increases;

(4) the mixed layer equivalent potential temperature and total water specific humidity are fairly independent of the divergence, except when the divergence is very small, but both are greater with a higher sea surface temperature;

(5) in order to obtain a positive jump in equivalent potential temperature, the sea surface temperature has to be colder than 16–17°C. A stratocumulus-topped mixed layer with negative $\Delta\theta_e$ is possibly unstable (see Lilly (1968) and § 4.4) This result is obviously dependent on the value chosen for the overlying stable layer temperature. Schubert uses values determined from the mean July 1967–70 Oakland sounding;

(6) the fluxes $\overline{w'\theta_e'}$ and $\overline{w'q_w'}$ are fairly independent of the divergence but increase rapidly as the sea surface temperature increases. These fluxes of conservative

quantities are continuous across the cloud base. However, the heat flux $\overline{w'\theta_e'}$, the water vapour flux $\overline{w'q'}$ the cloud water flux $\overline{w'c'}$ and the buoyancy flux $\overline{w'\theta_v'}$ are all discontinuous across $z=z_c$.

(7) somewhat surprisingly, the buoyancy flux is negative below cloud base. This means that on average upward moving air is virtually colder than downward moving air at the same height. The convective motion must be driven by the associated pressure field.

3.2.10 Horizontally Inhomogeneous, Steady State Solutions

The system (M.1)-(M.12) can be solved for the dependent variables under conditions of spatially varying external parameters such as sea surface temperature. The results can be interpreted in a Lagrangian sense, that is as the rate of change following a fluid parcel, or in an Eulerian sense with a locally steady state and d/dt interpreted as $V\partial/\partial x$.

The finite difference procedure used by Schubert et al (1977) to numerically integrate their 1-d model was a fourth order Runge-Kutta scheme. The model variables were initialized with the relevent steady state horizontally homogeneous solution.

The response of the varables to changing sea surface temperature downstream was found by Schubert to be towards the steady state values for the changed conditions. However, the adjustment was not found to be instantaneous; the lag was most pronounced for the mixed layer height h. The only variable to show any marked dependence on the large scale divergence in the spatially homogeneous solution was h. It is, therefore not surprising that there was practically no variation in any model variable except h when the boundary layer air moves to areas of different divergence. The adjustment of h was again found to be slow.

3.2.11 An assessment of 1-d models

It is clear from the work of Schubert described in the preceeding sections that a 1-d model adequately represents the general features of an unbroken stratocumulus layer. The comparisons of theory with observations made by Deardorff (1976b) also seem reasonable. In this comparison values of quantities on both sides of the equation

$$\frac{dh}{dt} - w_h = \frac{\left\{K_1\left(\overline{w'\theta_e'}\right)_0 - K_2\,\theta_0\left(\overline{w'q_w'}\right)_0 + \left[K_3 + \frac{(1-k)r}{2k}C_2\right]\frac{\Delta R}{\rho_h}\right\}}{\left\{\left[K_3 + \frac{(1-k)}{2k}C_2\right]\Delta\theta_e - \left[K_4 + \frac{(1-k)}{2k}\right]\theta_0\,\Delta q_w\right\}},$$

which is derived from (M.12), (M.8) and (M.9), were estimated from observations.

However the assumptions made in formulating a 1-d model limit its validity, particularly in circumstances where there is reason to suppose that the boundary layer is not well mixed. Such is the case when the stratocumulus layer is breaking up due to pockets of dry entrained air permeating the cloud when $\Delta\theta_v < 0$.

4. THREE DIMENSIONAL SIMULATIONS

Three dimensional simulations are motivated by the desire to investigate the vertical structure of quantities, such as the fluxes of heat and mosture, which have

to be parametrized in 1-d and large scale models. Observations of such quantities are scarce for cases when boundary layer clouds are present. A 3-d model of a stratocumulus-topped boundary layer has been developed and used for simulations by Deardorff (1976a and other paper cited therein.)

4.1 A description of the three dimensional model

Deardorff (1976a) gives a brief description of his model. Essentially it is based on the set of equations for a moist atmosphere in which only anelastic motion can take place.

With the anelstic approximation the continuity equation is

$$\nabla.\underline{v} = \frac{gw}{(\gamma-1)c_p\theta_o P_o} + \frac{w}{\theta_o}\frac{d\theta_o}{dz} \qquad (4.1)$$

$\theta_o(z)$ is a basic state potential temperature and $dP_o/dz = -g/c_p\theta_o$. The specific humidity q and the cloud water concentration c satisfy

$$\frac{\partial q}{\partial t} + \underline{v}.\nabla q = -S \qquad (4.2)$$

$$\frac{\partial c}{\partial t} + \underline{v}.\nabla c = S \qquad (4.3)$$

respectively. S is the microphysical source term for cloud water. It is assumed that no precipitation of cloud water takes place so there is no need for a rainwater variable. The momentum equation is

$$\frac{\partial \underline{v}}{\partial t} + \underline{v}.\nabla\underline{v} = -c_p\theta_o\nabla P_1 + g\underline{k}\left(\frac{\theta_1}{\theta_o} + 0.61q - c\right) - f\underline{k}\wedge\underline{v} \qquad (4.4)$$

The Exner variable $P=(p/p_r)^{R/c_p}$ has been used and written as $P = P_o(z) + P_1$. θ_1 is the deviation of the potential temperature from the basic state ie. $\theta = \theta_o(z) + \theta_1$. Lastly the thermodynamic equation is

$$\frac{\partial\theta}{\partial t} + \underline{v}.\nabla\theta = \frac{1}{c_p P_o}(Q + LS) \qquad (4.5)$$

where Q is the source of radiational heat and L is the latent heat of water.

Averaged over a grid volume of the numerical model (4.2)-(4.5) become respectively:

$$\frac{\partial q}{\partial t} + \underline{v}.\nabla q = -S - \frac{1}{\rho_o}\nabla.(\rho_o\overline{\underline{v}'q'}) \qquad (4.6)$$

$$\frac{\partial c}{\partial t} + \underline{v}.\nabla c = S - \frac{1}{\rho_o}\nabla.(\rho_o\overline{\underline{v}'c'}) \qquad (4.7)$$

$$\frac{\partial \underline{v}}{\partial t} + \underline{v}.\nabla\underline{v} = -c_p\theta_o\nabla P_1 + g\underline{k}\left(\frac{\theta_1}{\theta_o} + 0.61q - c\right) - f\underline{k}\wedge\underline{v} - \frac{1}{\rho_o}\nabla.(\rho_o\overline{\underline{v}'\underline{v}'}) \qquad (4.8)$$

$$\frac{\partial \theta}{\partial t} + \underline{v}.\nabla\theta = \frac{1}{c_p \rho_o}(Q+LS) - \frac{1}{\rho_o}\nabla.(\rho_o \overline{\underline{v}'\theta'}) \qquad (4.9)$$

The overbar denotes the grid volume mean (it has been left off the basic variables for convenience) and the prime denotes a deviation from this mean. Note that the averaging involved in (4.6)–(4.9) is not the same as in the equations in § 3.

Deardorff introduces the total liquid water concentration q_w (as defined in § 3.1) and the liquid water potential temperature θ_l given by

$$\theta_l = \theta - \frac{Lc}{c_p \rho_o} .$$

Like the equivalent potential temperature θ_e, θ_l is conserved during phase changes. The prognostic equations for q_w and θ_l are

$$\frac{\partial q_w}{\partial t} + \underline{v}.\nabla q_w = -\frac{1}{\rho_o}\nabla.(\overline{\rho_o \underline{v}' q_w'}) \qquad (4.10)$$

$$\frac{\partial \theta_l}{\partial t} + \underline{v}.\nabla\theta_l = -\frac{1}{\rho_o}\nabla.(\rho_o \overline{\underline{v}'\theta_l'}) \qquad (4.11)$$

Using the values of q_w and θ_l computed from (4.10) and (4.11) the values of and q, c, θ can be diagnosed using the method presented in Sommeria and Deardorff (1977). Hence the buoyancy $\theta_v = \theta_l + \theta_o(0.61q - c)$ is known for use in the equation of motion (4.8).

Even though Deardorff's grid spacing of 50m allows most of the eddies to be resolved, he takes account of fluxes due to sub-grid scale motions. Earlier versions of his model included the full set of prognostic equations for the second order correlations. However, no deterioration in results were obtained when he used a single prognostic equation for the turbulent kinetic energy. This equation is (cf (3.17)):

$$\frac{D\bar{E}}{Dt} = \frac{1}{\rho_o}\nabla.(\rho_o K_m \nabla \bar{E}) + \tfrac{1}{2} K_m\left(\frac{\partial v_i}{\partial x_j} + \frac{\partial v_i}{\partial x_j}\right)^2 + \frac{g}{\theta_o}\overline{w'\theta_v'} - \frac{c_\varepsilon \bar{E}^{3/2}}{l} \qquad (4.12)$$

diffusion | mechanical generation | generation due to buoyancy | dissipation

The turbulent fluxes are given by

$$\overline{v_i' v_j'} = \tfrac{2}{3}\bar{E}\,\delta_{ij} - K_m\left(\frac{\partial v_i}{\partial x_j} + \frac{\partial v_j}{\partial x_i}\right) \qquad (4.13a)$$

$$\overline{v_i' q_w'} = -\left(\frac{K_h}{K_m}\right) K_m \frac{\partial q_w}{\partial x_i} \qquad (4.13b)$$

$$\overline{v_i'\theta_l'} = -\left(\frac{K_h}{K_m}\right) K_m \frac{\partial \theta_l}{\partial x_i} \qquad (4.13c)$$

where $K_m = 0.1 \bar{E}^{1/2} l$ and $\frac{K_h}{K_m} = 1 + \frac{2l}{\Delta}$.

Δ is the grid spacing and l is a small-scale mixing length which Deardorff takes as

$$l = \min\left\{\Delta,\ 0.76\bar{E}^{1/2}/\left(-\frac{g}{\theta_0}\overline{w'\theta_v'}\right)^{1/2}\right\} \quad \text{when } \overline{w'\theta_v'} < 0 \quad \text{(stable)}$$

and $l = \Delta$ when $\overline{w'\theta_v'} \geq 0$ (unstable or neutral)

With c_E specified as

$$c_E = 0.188 + 0.512\, l/\Delta$$

there is a critical value of the Local Richardson number of 0.2.

The expression for the subgrid-scale buoyancy flux $\overline{w'\theta_v'}$ in terms of $\overline{w'q_w'}$ and $\overline{w'\theta_l'}$ depends on whether the air is saturated or not. Equations of the form of (3.25) have to be used. The effect of subgrid-scale condensation could be included in the model by the method presented in Sommeria and Deardorff (1977).

The finite differencing used by Deardorff is of an energy conserving flux form. A space staggered grid is used ensuring second order accuracy for the spatial derivatives. 40^3 grid points are used in a domain 2km x 2km x 2km. The time step is about 5 seconds. In the simulations run by Deardorff lateral boundary conditions were cyclic, w=0 at each grid point at the lower horizontal boundary and at the height z = 2km. Turbulent fluxes at the surface were found from a calculated time-dependent ground temperature, soil moisture and a specified roughness length.

4.2 Simulation with stratocumulus throughout the mixed layer

Deardorff integrated one case where the air was so moist that the condensation level was, on average, only 0.1h, where h was the mixed layer height. Radiative cooling was imposed at a rate of -1.5×10^{-3} Ks^{-1} within the uppermost saturated grid volume (which has a height of 50m). Horizontal means taken over the model domain were calculated for the quantities q_w, θ_e, θ_l, θ_v, c and the fluxes $w\theta_v$ and $w\theta_e$. The fluxes included the subgrid-scale contributions, as well as those on the resolvable scale. With $\langle\ \rangle$ denoting the horizontal mean the main features which emerged from the simulation include:

(1) nearly uniform values of the conservative quantities $\langle\theta_e\rangle$, $\langle\theta_l\rangle$ and $\langle q_w\rangle$ in the lower 85% of the mixed layer. However $\langle q_w\rangle$ and $\langle\theta_l\rangle$ had poorly mixed shoulders

in the top 15%. The well-mixed hypothesis used in § 3.2.1 for the 1-d model is therefore well confirmed for θ_e but is not so good for q_w;
(2) a moist adiabatic lapse rate for $\langle\theta_v\rangle$ within the stratocumulus layer;
(3) a linearly increasing liquid water content $\langle c\rangle$ from cloud base to about 0.85h but a marked falling off from 0.85 h to h. It is this which probably "causes" the rounded shoulder shape of the $\langle q_w\rangle$ and $\langle\theta_l\rangle$ profiles in the top 15%. This sort of vertical profile of $\langle c\rangle$ is also a feature of observations (see § 2.1);
(4) negative jumps in $\langle w\theta_e\rangle$ and $\langle w\theta_v\rangle$ at z =h due to radiative flux divergence. If the cloud top had no undulations so that all the radiative cooling took place between h-50m and h the jump in $\langle w\theta_e\rangle$ would be 50m x -1.5×10^{3} Ks^{-1} = $-7.5 cm^{-1}$ K. However the simulation gives a jump of about 0.3 of this value. This indicates that most of the cooling occurs in the cloud domes penetrating into the inversion layer just above z = h. Thus a suitable value for the factor r introduced in § 3.2.1 might be 0.7.

These features are summarised in Figure 4 which is taken from Deardorff (1976a)

4.3 Simulation with stratocumulus in the upper mixed layer

In Deardorff's second simulation the moisture content of the mixed layer was reduced so that the cloud base was approximately at half the mixed layer height. The jump of $\langle w\theta_v\rangle$ at cloud base as described in § 3.2.6 becam clearly evident. As in the previous simulation there was a double jump structure for $\langle w\theta_e\rangle$ and $\langle w\theta_v\rangle$ in the neighbourhood of z =h. Figure 5 taken from Deardorff (1976a) shows these features.

The vertical profiles of the variables and fluxes as found in Deardorff's 3-d simulations in general confirm the assumptions made in the 1-d model described in § 3. As for the entrainment hypothesis, the results indicate that the negative area extending to the top of the top of the turbulent region (on a plot of $\langle w\theta_v\rangle$ against z) is a fairly constant proportion of the positive area below. This is what the theoretical discussion in § 3.2.6 suggested. The factor (1-f) was found by Deardorff to be 0.07 ± 0.022. $\langle w\theta_v\rangle_h$ was found to be 1.1 $\langle w\theta_v\rangle_{mean}$ giving a value of the entrainment parameter k of 0.35.

The turbulent kinetic energy balance in the simulations confirmed that the wind-shear source term is negligible and that the main balance is between dissipation and generation due to buoyancy. This gives further credence to the argument leading to the entrainment hypothesis in § 3.2.6.

4.4 Simulation of a breaking stratocumulus layer

In § 3.2.11 the limitation on the validity of 1-d models when the well-mixed assumption breaks down was discussed. Since no such assumption is made in a 3-d model it can be used to simulate the break up of a stratocumulus layer. Deardorff (1976a) presents some results for such a situation. He started the integration with $\Delta\theta_e$ positive but only a few degrees in magnitude and then reduced it in small steps. When $\Delta\theta_e < \theta_c(C_1\Delta q + \Delta c)$ it can be argued that pockets of dry

air can permeate the cloud layer and lead to its gradual break-up.

After $\Delta\theta_e$ fell below -1K the entrainment rate We increased significantly, but not catastrophically, and increasing amounts of unsaturated air became evident in the cloud layer. Most of the drying out occurred near cloud base. Deardorff could not carry the integration on towards a scattered cumulus layer because the top of the boundary layer reached too close to the top of the model.

The profile of $\langle\theta_v\rangle$ evolved from the moist adiabatic lapse rate towards the dry adiabatic lapse rate. q_w did not remain well mixed, ie $\langle q_w\rangle$ did not remain constant with height. θ_e did remain well mixed. The break down of the well mixed assumption for q_w became most clearly evident in the profile of $\langle wq_w\rangle$ which was not linear. The flux of total water was enhanced in the upper part of the cloud layer as soon as significant gaps in the cloud layer appeared. This is consistent with the drying in the base and middle of the cloud layer.

4.5 Conclusions

The implications of the 3-d simulations for the parameterization of cloud topped mixed layers are that the well mixed assumption for moisture should not be made unless the cloud layer is solidly saturated and that this is unlikely to be the case when $\Delta\theta_e$ drops below about -1K. Therefore the 1-d model of § 3.2 is not suitable for the study of a breaking cloud layer.

Parameterisation of the mixed layer growth rate when there are scattered cumuli growing out of its top has been developed (see § 5 of Deardorff (1976a) for a review). The essential difference between this case and that of a clear mixed layer is an additional cloud-induced subsidence. Theories have yet to be put forward for the intermediate case of broken stratocumulus. It would seem to be a crude method to interpolate between the cases of solid saturation and scattered cumuli.

The simulation of the transition from scattered cumuli to a stratocumulus layer does not seem to have been attempted. With regard to this, it is planned to use the Met O 11 non-hydrostatic mesoscale model to study the effect of cumulus activity on the boundary layer structure.

REFERENCES

Cornford S G (1966) Stratocumulus – A review of some Physical Aspects. Met Mag 95, 292.

Deardorff J W (1976a) Clear and Cloud-Capped Mixed Layers: Their Numerical Simulation, Structure and Growth and Parameterisation ECMWF Seminars on the Treatment of the Boundary Layer in Numerical Weather Prediction pp 234–284.

Deardorff J W (1976b) On the Entrainment Rate of a Sc-Topped Mixed Layer Quart J Roy. Met. Soc 102, 563.

Findlater J (1961) Thermal Structure in the Lower Layers of Anticyclones. Quart J Roy Met Soc 87, 513.

James D G (1959) Observations from Aircraft of Temperatures and Humidities near Stratocumulus Cloud. Quart J Roy Met Soc 85, 120.

Lilly D K (1968) Models of Cloud-Topped Mixed Layer under a strong inversion. Quart J Roy, Met Soc 94, 292.

Moore J G (1964) Some further observations from aircraft of temperature and humidities near stratocumulus cloud. Scient. Pap Met Off London 19.

Schubert W H (1976) Experiments with Lilly's Cloud-Topped Mixed Layer Model. J Atmos Sci 33, 436.

Schubert W H, Wakefield, J S, Steiner, E J & Cox S K (1977) Marine Stratocumulus Convection. Dept Atmospheric Science, Colorado State University Paper no 273.

Sommeria G and Deardorff J W (1977) Subgrid-Scale Condensation in Models of Non-precipitating Clouds. J Atmos Sci 34, 344

Stull R B (1976) The Energetics of Entrainment Across a Density Interface. J Atmos Sci 33, 1260.

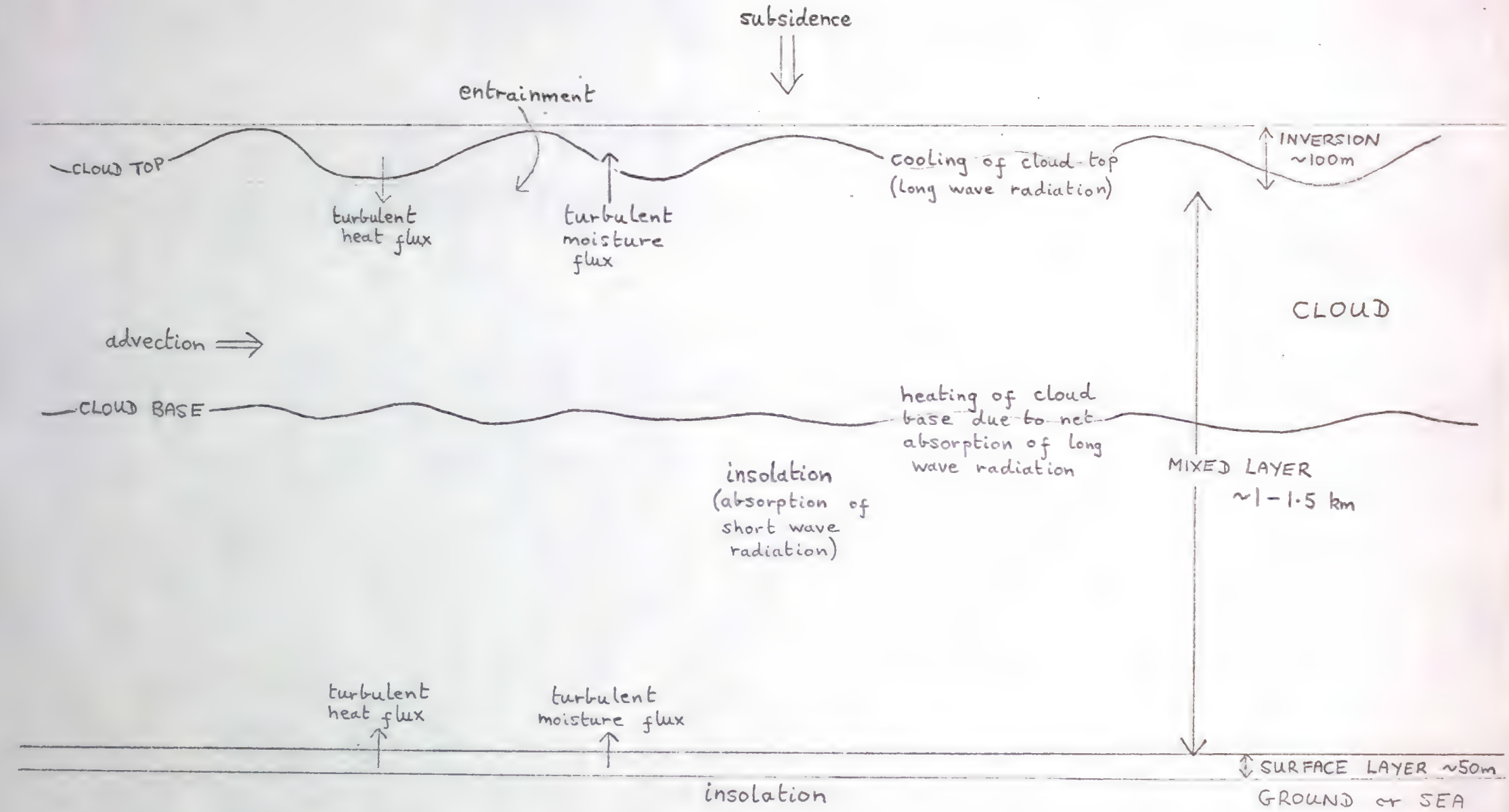

FIGURE 1.

The general balance of physical processes in and near stratocumulus cloud.

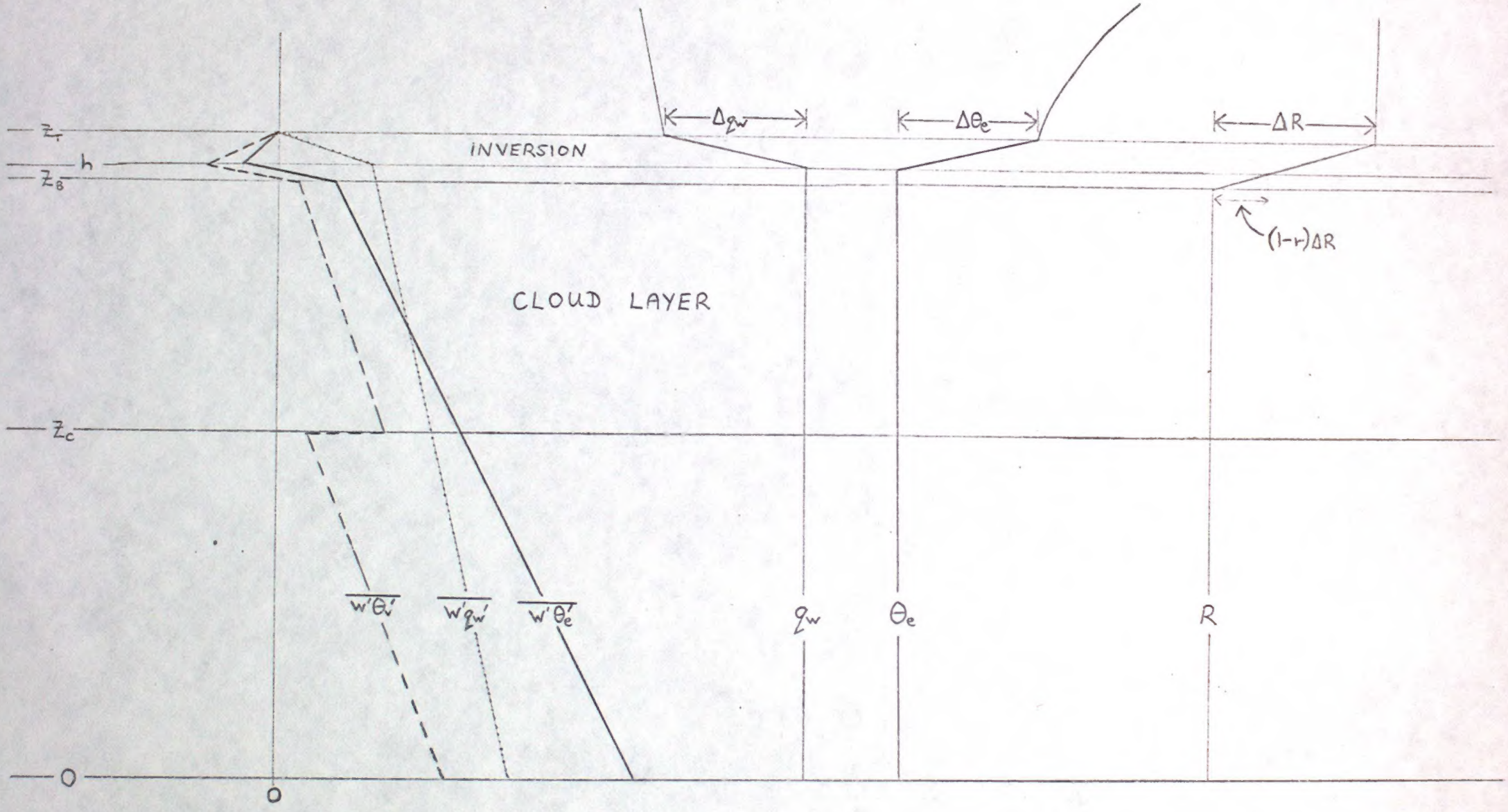

FIGURE 2.

Idealised vertical profiles of q_w, θ_e, R, $\overline{w'\theta_e'}$, $\overline{w'q_w'}$ and $\overline{w'\theta_v'}$ assumed for the model of § 3.

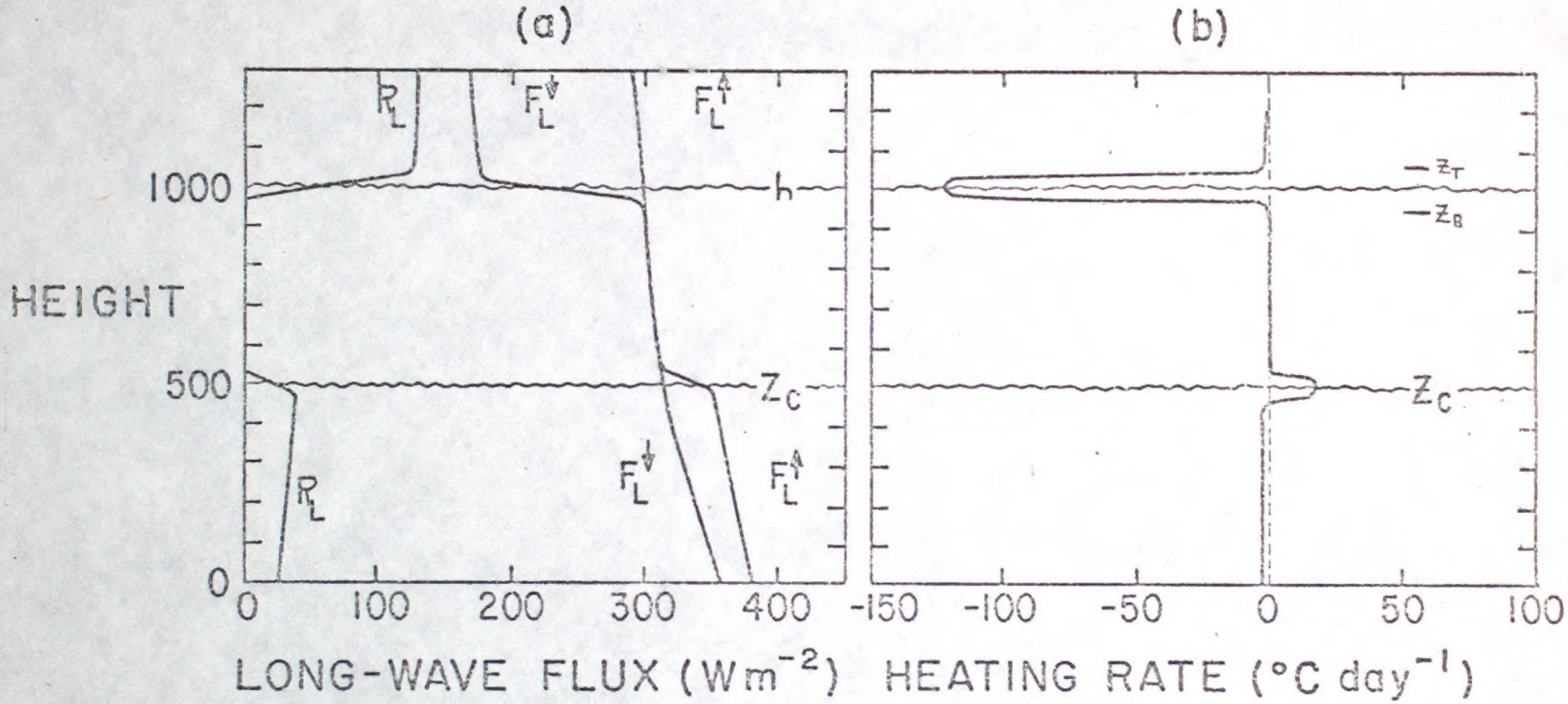

(a) Idealized profiles of the upward and downward long-wave radiative fluxes in and near a stratocumulus cloud. (b) Resulting heating rate. Values on the abscissa and ordinate are meant to be only roughly indicative. The warming at cloud base and the cooling in the subcloud layer are neglected in the present model.

FIGURE 3.

(Taken from Schubert et al. (1977))

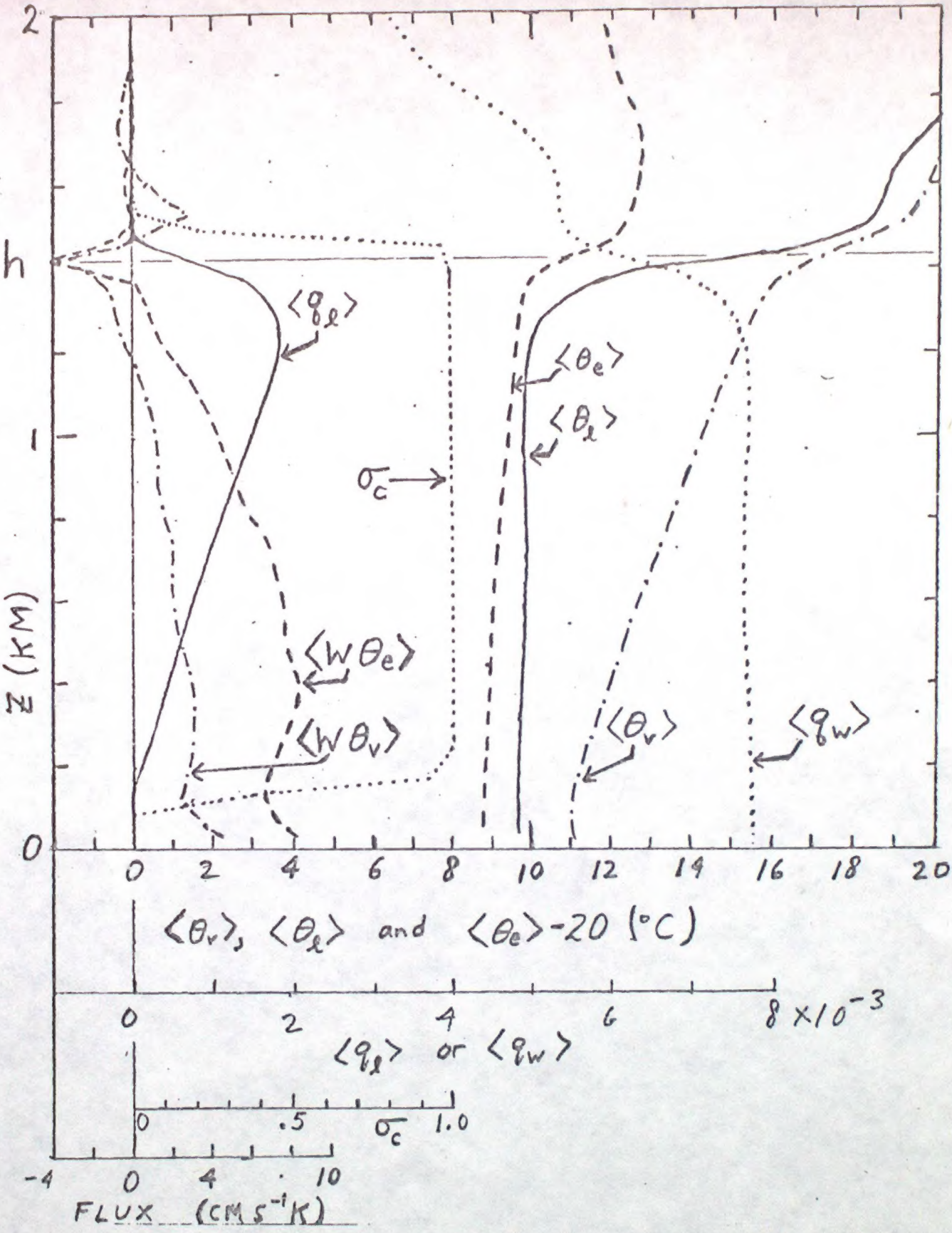

Profiles of the horizontally averaged quantities: $\langle \theta_v \rangle$, $\langle \theta_\ell \rangle$, and $\langle \theta_e \rangle$ in degrees C, upper abscissa; $\langle q_\ell \rangle$ and $\langle q_w \rangle$, second scale at bottom; fraction of area saturated at a given height, σ_c, third scale; and the fluxes $\langle w\theta_v \rangle$ and $\langle w\theta_e \rangle$, lowermost scale, existing at a particular time. Cloud base is at about 120m and cloud top at 1400m.

FIGURE 4.

(Taken from Deardorff (1976a)

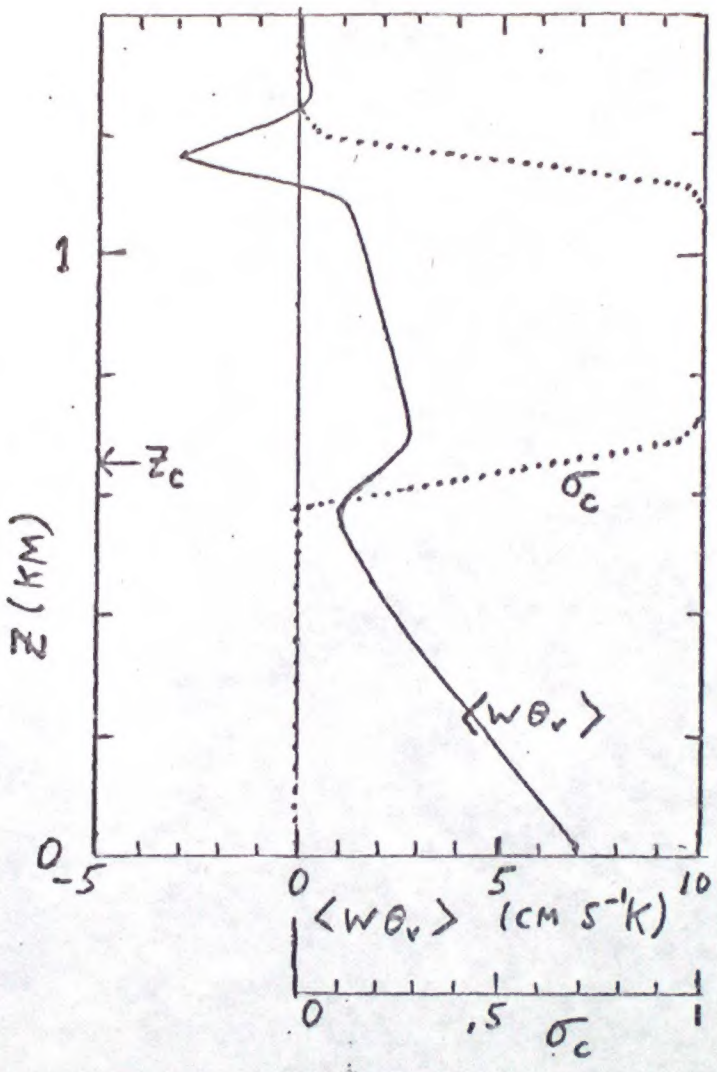

Vertical profiles of $\langle w\theta_v \rangle$ and local cloud fraction, σ_c, for the case of stratocumulus in the upper half of the mixed layer. The averaging is over a time period of 0.32 hrs.

FIGURE 5.

(Taken from Deardorff (1976a))